

## Mechanical Size Effect of Freestanding Nanoconfined Polymer Films

Guorui Wang,<sup>||</sup> Farzin Najafi,<sup>||</sup> Kevin Ho, Mahdi Hamidinejad, Teng Cui, Gilbert C. Walker,\*  
Chandra Veer Singh,\* and Tobin Filleter\*



Cite This: *Macromolecules* 2022, 55, 1248–1259



Read Online

ACCESS |



Metrics & More

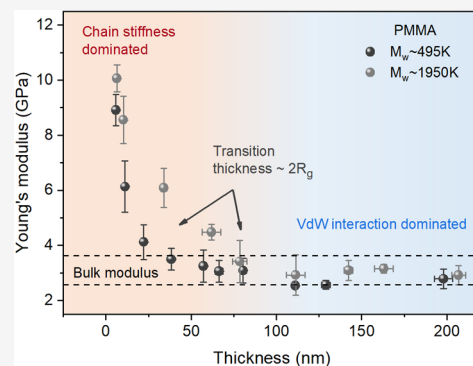


Article Recommendations



Supporting Information

**ABSTRACT:** While elastic properties of nanoconfined polymer films have been recognized to show departures from bulk behavior, a careful understanding of the origins of mechanical size effects remains weak. Here, we report a significant mechanical stiffening of freestanding ultrathin poly(methyl methacrylate) films of varying thicknesses (6–200 nm) through atomic force microscopy deflection measurements at ambient conditions. After excluding the substrate influence, the stiffening mechanism is linked to extended chain conformations based on small-angle X-ray scattering and infrared nanoscopic characterization. We advocate that the entropic elasticity of individual chains plays a significant role in polymer mechanics in nanoscale thickness films, where the entanglement density is apparently low, with chains oriented in the plane of the film, unlike a bulk polymer. Molecular dynamics simulations further unveil the dominance of entropic contributions over enthalpic contributions to the chain stiffness that endows polymer films with higher load-bearing capacity and accounts for the stiffening at the nanoscale. The results presented herein provide a mechanistic understanding of molecular origins of the size effect, serving as a potent design strategy for accessing high-performance polymer-based devices.



### INTRODUCTION

Polymers are critical components in a myriad of applications such as flexible electronics, composites, and sensors, especially with growing needs for ever-shrinking dimensions.<sup>1–3</sup> Understanding the mechanical properties of nanoconfined polymer films is essential to predict and advance device performance and reliability. As the characteristic dimensions downscale to nanometers, it has been acknowledged that the mechanical behavior of nanomaterials differs dramatically from that of bulk materials.<sup>4</sup> This observation, termed as a size effect, is now well known in metals; however, it is still ambiguous for polymers.<sup>5</sup> In particular, Young's moduli of polymer films have been reported to exhibit conflicting thickness dependency. For example, while nanoindentation tests found an increase in modulus under nanoconfinement, surface wrinkling measurements showed an elastic softening with decreasing thickness.<sup>6–9</sup> Such softening behaviors were also observed during uniaxial tensile deformation via molecular dynamics (MD) simulations.<sup>10,11</sup> In contrast, a macroscopic uniaxial tensile experiment of freestanding polymer films has recently demonstrated a constant elastic modulus with varying thickness, which was found to depend on the measurement strain rate.<sup>12–14</sup> Unfortunately, the molecular-level mechanisms underlying such contradictory observations are still not well understood.

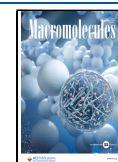
In principle, the mechanical properties of polymer materials are controlled by chain conformations and architectures at a microscopic level.<sup>15</sup> For a glassy polymer with randomly coiled

molecules, the main contribution to its Young's modulus derives from intermolecular van der Waals (vdW) interactions between neighboring chains, which explains why most macroscopic amorphous polymers have elastic moduli in a close range of 2–4 GPa.<sup>16</sup> When subjected to a geometrical confinement in the thickness direction, a reduction in chain entanglements has been observed in films, especially near the surface due to the excluded volume effect.<sup>17,18</sup> In terms of fewer entanglements and higher mobility of polymer chains, there has been a growing awareness that chain stiffness is playing a more significant role in the response of ultrathin polymer films to mechanical loading.<sup>19,20</sup> Thus, the exploration into microscopic details of the deformation process involving the individual chain mechanics deserves careful attention and the nature of the chain stiffness should be first elucidated. Referring to the elasticity of single chains, earlier works have highlighted two events that take place during their tensile deformation: entropic elasticity due to the conformational restriction and enthalpic/energetic elasticity related to the backbone straining.<sup>21</sup> However, it remains an open question as to which one of these phenomena would dominate the elastic

**Received:** November 9, 2021

**Revised:** January 13, 2022

**Published:** February 9, 2022



behavior of nanoconfined films. The competitive interplay between entropic and enthalpic contributions to the single-chain stiffness hence calls for further study under nanoconfinement.

Another issue worthy of close scrutiny is whether the change in measured properties essentially reflects a size effect or results from a substrate effect that is conceivably magnified by the reduction of film thickness.<sup>7,22,23</sup> On the one hand, the stress field under the tip is found to propagate far into the substrate even for small indentation depth, resulting in a convolution of measurements with substrate effects.<sup>24</sup> This leads to, more accurately, the so-called “indentation size effect” that depends more upon extrinsic factors such as indentation depth, tip shape/bluntness, and interfacial interactions.<sup>25</sup> In this context, Li et al. modified the contact mechanics model through finite element simulations of nanoindentation experiments to separate the substrate effect from the thickness-dependent modulus of polymer films and observed a softening behavior that agreed with wrinkling measurements.<sup>26</sup> However, in addition to changing the localized stress state, the substrate also interacts with polymer chains and restricts their molecular mobility near the interface, thus accounting for the elevated glass-transition temperature ( $T_g$ ) and mechanical stiffening of polymer films.<sup>7,27</sup> Toward this end, of crucial importance is to experimentally preclude the substrate influence to reveal the true mechanical response of molecular structures and the intrinsic nature of the size effect at the nanoscale.

Herein, we report a mechanical stiffening behavior of freestanding polymer films in confined geometry through atomic force microscopy (AFM) deflection testing. Through a combination of small-angle X-ray scattering (SAXS) and infrared nanospectroscopic measurements, a transition in chain conformations was identified from bulk to ultrathin film, which can be directly related to the mechanical behavior of the polymer films. Molecular dynamics (MD) modeling was performed to gain deeper insights into the atomistic stiffening mechanisms and highlight the contribution of individual chains. By separating the force origins originating from the backbone straining and conformational transition, the enthalpic and entropic contributions to the single-chain stiffness were examined in detail for the first time. In comparison with previous studies on the mechanical measurement of polymer ultrathin films, this work brings a clearer picture of understanding a generalized size effect at the nanoscale.

## METHODS

**Preparation of Freestanding Polymer Films.** Poly(methyl methacrylate) (PMMA,  $M_w = 495$  kg/mol, PDI = 1.1 and  $M_w = 1950$  kg/mol, PDI = 1.3) was dissolved in anisole and then spin-coated on a silicon wafer. The film thickness was controlled via solution concentration (0.1–2.0 wt %) and spin speed (1000–4000 rpm). Following the method as previously reported,<sup>28</sup> a detachment of the PMMA film from the initial surface was achieved by partially etching the surface of SiO<sub>2</sub> with 1 M NaOH aqueous solution. During the etching, silicon wafer was kept floating on the solution surface and avoided NaOH interacting with PMMA. Thin films were rinsed in DI water immediately after the detachment, minimizing the impact of NaOH on PMMA properties. Finally, PMMA films were successfully transferred onto another silicon wafer patterned with circular microwells (diameter of  $\sim 1.5$   $\mu\text{m}$ ) and then dried for 30 min at 80 °C (Figure S1). Subsequent vacuum annealing was performed at 120 °C (above bulk  $T_g$  of  $\sim 110$  °C) for 2 h to increase the adhesion

between the film and surface, as well as remove the residual solvent and stress.

**Measurement of Glass-Transition Temperature.** PMMA thin films were transferred onto a silicon TEM grid with a square window of 500  $\mu\text{m}$  (silicon nitride membrane removed). Jobin-Yvon Uvisel spectroscopic ellipsometer equipped with a hot plate in air was used to probe the  $T_g$  for ultrathin freestanding PMMA films. The ellipsometric scan was conducted with radiation having a wavelength of 387.5 nm and an angle of incidence of 70°. The ellipsometric angles ( $\varphi$  and  $\Delta$ ) were continuously monitored, while the sample temperature was increased from room temperature up to 130 °C with an increment of 2.5 °C. The ellipsometric angles were recorded after the temperature stabilized in 2 min. A plot of  $\varphi$  versus temperature was generated to observe a change in slope at  $T_g$ .

**Measurement of Young's Modulus.** AFM deflection testing on freestanding polymer films was conducted at ambient conditions using a commercial AFM system (Asylum Research, MFP-3D). A diamond AFM probe (Nanoscience Inc., ND-DYI Series) was utilized, and the spring constant of the cantilever was calibrated to be 31.1 N/m.<sup>29</sup> The tip radius was measured to be  $\sim 100$  nm by scanning electron microscopy (SEM, Hitachi SU3500). Before each indentation, the samples were scanned in a tapping mode to locate a freestanding area over the hole. Then, the AFM tip was centered in the middle of the circular hole and the film was loaded up to 200 nN in contact mode. The indentation rate was set as 1  $\mu\text{m/s}$  to minimize any viscoelastic effect. After indentation, AFM topography imaging was performed, showing no residual impression or damage, to ensure elastic deformation of deflected films (Figure S3). In addition, no significant hysteresis was observed when comparing the loading and unloading curves (Figure S4), signifying that no significant slippage occurred between PMMA film and silicon substrate.<sup>30</sup> The force versus displacement curves were finally obtained to quantitatively determine the modulus of polymer films.

**Characterization of Polymer Chain Conformation.** Small-angle X-ray scattering (SAXS) experiments were carried out using Anton Paar SAXSpace, configured in a beam collimation mode. Silicon wafers coated with PMMA films were affixed to a sample holder, which allows the incident X-ray beam oriented nearly parallel to the film edge and then exposed for 30 min to the rays at 140 °C. The measurements were executed in vacuum to prevent X-ray damage. Scattering curves were obtained in the  $q$ -range between 0.1 and 1.5  $\text{nm}^{-1}$ , assuming that  $q$  is the scattering vector and  $2\theta$  is the scattering angle ( $q = 4\pi \sin \theta / \lambda$ ). The background scattering was collected using a bare silicon wafer as a control, as shown in Figure S10. The infrared (IR) nanoimaging experiments were performed in ambient conditions by scanning near-field optical microscopy (SNOM) and peak force infrared microscopy (PFIR), equipped with a daylight solution quantum cascade laser. The SNOM is performed by AFM (Bruker Inspire) using a platinum/iridium-coated tip (NanoWorld Arrow-NCpt) with curvature radius  $< 25$  nm, operating in the tapping mode with a resonance frequency of approximately 285 kHz.<sup>31</sup> PFIR is performed using a custom-modified Bruker Inspire in a peak force quantitative nanomechanical mapping (QNM) mode with a platinum/iridium-coated tip (NanoWorld Arrow-NCpt). Tip deflection curves are collected using a data acquisition card (National Instruments PCI-5122) and processed to display the PFIR spectra with a LabView program.

**MD Modeling and Simulations.** Monodisperse PMMA chains with 200 repeating units ( $M_w = 20$  025.4 g/mol) were packed into a tetragonal box with in-plane dimensions of 30  $\times$  30  $\text{nm}^2$ . For the confined film system, periodic and fixed boundary conditions were applied in in-plane and thickness directions, respectively, while a periodic boundary condition was applied for all three directions of the bulk system. The fixed boundary prevents the polymer chains from passing freely in the thickness direction and preserves the straight conformations of the chains prior to the thermal relaxation and quenching processes. A similar simulation setup with box creation methods has been reported on ultrathin polymer films.<sup>6,32,33</sup> A bulk algorithm without constraint in the thickness direction was used to create a 20 nm thick sample to represent the bulk polymer

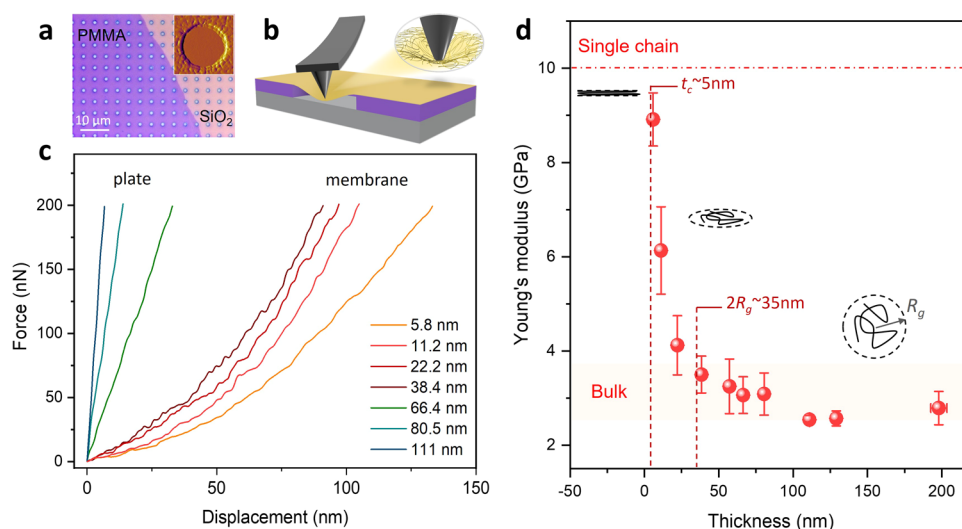


**Figure 1.** AFM deflection measurement of freestanding PMMA films. (a) Optical image of an 11.2 nm thick PMMA film (purple region) deposited on silicon wafer patterned with circular microwells. The inset is the AFM amplitude image showing the flat freestanding area. (b) Schematic illustration of the AFM deflection testing setup. (c) Typical force–displacement curves showing a plate-to-membrane transition in deformation with a decreasing thickness of PMMA. (d) Thickness-dependent Young's moduli of freestanding PMMA films. The shadowed region shows the bulk value range based on the literature,<sup>44,45</sup> while the horizontal dot-dashed line indicates the previously reported single-chain modulus.<sup>46</sup> Vertical dashed lines denote the critical thickness corresponding to the change of chain conformations.  $R_g$  is the radius of gyration that describes the dimensions of polymer chains in the amorphous bulk state, and  $t_c$  is the critical thickness below which polymer chains are extended and oriented parallel to the surface.

configuration. The systems were modeled by an all-atom approach containing 540–1080 K atoms. The DREIDING forcefield that shows high accuracy in the mechanical study of polymer systems was employed to perform the MD simulations.<sup>34,35</sup> MD simulations were carried out using open-source large-scale atomic/molecular massively parallel simulator (LAMMPS) software,<sup>36</sup> and open visualization tool (OVITO) was used to visualize the results.<sup>37</sup> Time steps of 0.5 and 1.0 fs were used for thin film and bulk systems, respectively. The cutoff radius for the Lennard-Jones (LJ) and Coulomb interactions was set equal to 1 nm. Random initial velocities were assigned to the systems using the Gaussian velocity distribution algorithm. To achieve a complete amorphous configuration, all systems were initially relaxed under isothermal and isobaric (NPT) ensemble at  $T = 500$  K (above the melting temperature) and  $P = 1$  atm for 0.4 ns. An LJ-type wall interaction was considered for top and bottom faces in the thickness direction. Nosé–Hoover thermostat and barostat with damping constants of 25 and 250 fs, respectively, were used to maintain constant temperature and pressure. Then, the systems were quenched from melt configuration at 500–300 K (room temperature) with a cooling rate of 4 K/ps to derive the final amorphous configurations. Considering the glass-transition temperature of 378 K for PMMA,<sup>38</sup> all systems were in glassy state with a final density of 0.93–1.0 g/cm<sup>3</sup>, which is consistent with values as reported in the literature.<sup>33,39</sup> Indentation tests were performed under an NVT ensemble by applying a displacement field to resemble the indenter. The indenter's velocity and radius were 0.00025 nm/ps and 3.5 nm, respectively. A circular region with a diameter of about 28 nm was selected at the center as the target film subjecting to deflection, while the rest of the atoms were fixed.

## RESULTS AND DISCUSSION

**Mechanical Properties of PMMA Films.** Poly(methyl methacrylate) (PMMA,  $M_w \sim 495$  K) films were transferred onto silicon wafers patterned with circular microwells, showing flatness within the suspended regions (Figure 1a). The thickness, measured by AFM tapping mode imaging, ranged from 5.8 to 198.0 nm (Figure S2). Mechanical properties were measured by AFM deflection testing with a diamond tip, as illustrated in Figure 1b. Representative force–displacement

( $F$ – $\delta$ ) curves are displayed in Figure 1c, where a transition from membrane behavior to plate behavior is observed with increasing thickness.<sup>40</sup> Considering a clamped, circular film with central point loading, the relationship between the applied force and resulting displacement can be approximated as<sup>40</sup>

$$F(\delta) = \frac{4\pi Et^3\delta}{3(1-\nu^2)a^2} + \pi\sigma_0\delta + \frac{Etq^3\delta^3}{a^2} \quad (1)$$

where  $F$  is the loading force,  $\delta$  is the deflection at the central point,  $E$  is Young's modulus,  $t$  is thickness,  $a$  is the microwell radius, and  $\sigma_0$  is the pretension in the film accumulated during preparation.  $q = 1/(1.05 - 0.15\nu - 0.16\nu^2)$  is a dimensionless constant determined by  $\nu$ , Poisson's ratio taken as 0.33 here.<sup>41</sup> Even though a decrease in Poisson's ratio was reported for ultrathin films compared with that of bulk polymers,<sup>42</sup> such a change is found to be insignificant for the interpretation of moduli extracted from AFM deflection testing.

The three terms on the right-hand side of eq 1 are assigned to bending, pretension, and stretching, respectively. In detail, for ultrathin film with thickness  $\leq 38.4$  nm, the bending stiffness (the first term) was found to be negligible so that the deformation is stretching-dominated and presents a cubic dependence in the  $F$ – $\delta$  curve. Recently, a theoretical study from Vella claimed that,<sup>43</sup> in the intermediate indentation regime, namely,  $\delta\sqrt{(Et/\sigma_0)}/a \sim O(1)$ , the use of sharp tips could induce considerable errors, while such an effect turns out to be negligible for shallow indentation depths. In the present work, the relatively large tip radius ( $R \sim 100$  nm) and fitting within a small range ( $\delta \sim 50$  nm) for membrane behavior are envisioned to yield more accurate estimates. For film thicknesses of 66.4 nm and higher, the bending stiffness contribution becomes dominant due to its cubic thickness dependence, and the  $F$ – $\delta$  curve becomes linear disregarding the third term. Note that the effect of pretension and the contact deformation has been considered to be negligible,

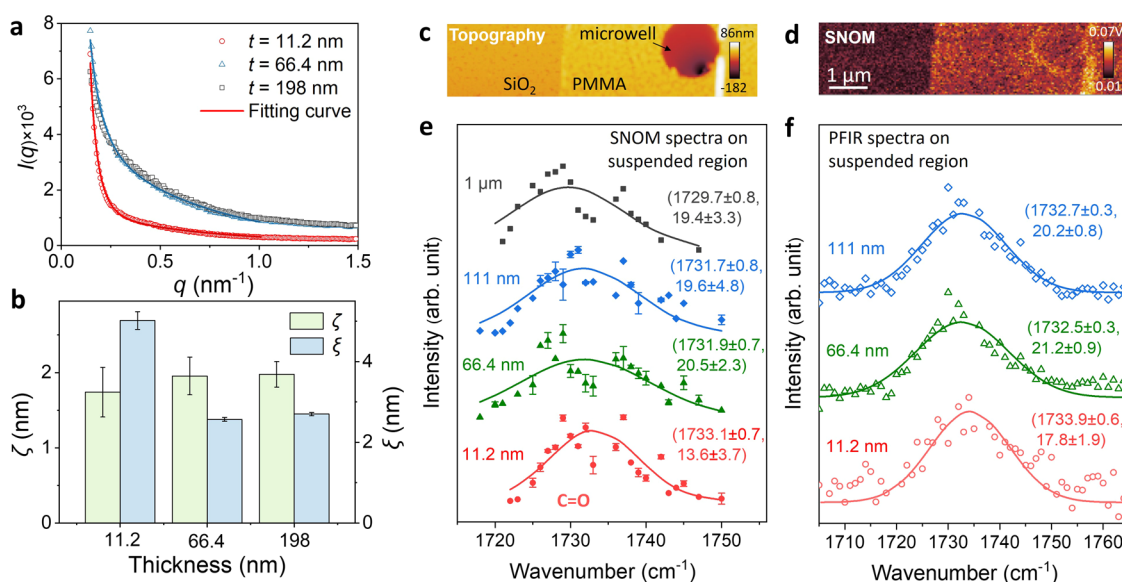


**Figure 2.** Characterization of molecular chain conformations in 495 K PMMA films. (a) SAXS results showing plots of  $I(q)$  as a function of  $q$  for PMMA films with different thicknesses. Solid curve is the fitting to the data based on eq 2. (b) Thickness dependence of fitting parameters. (c, d) AFM topography image of the PMMA thin film and corresponding SNOM image taken at 1730 cm<sup>-1</sup>. (e) SNOM and (f) PFIR spectra on resonance with the C=O stretch of the PMMA molecules in the suspended area for different thicknesses. The peak position and FWHM are labeled in parentheses.

emphasizing the reliability of the mechanics model (eq 1) in interpreting the elastic deformation of polymer films (see Supporting Information S1 and Figures S5 and S6).

Figure 1d presents the thickness dependence of Young's moduli for PMMA films. Above the thickness of 40 nm, the modulus average is around 3 GPa as anticipated and lies within a reasonable range as previously reported for bulk PMMA (shadowed region: 2.7–3.7 GPa).<sup>44,45</sup> When the film thickness drops below 20 nm, a precipitous increase is clearly visible in modulus, which can reach as high as  $\sim$ 9 GPa at  $t = 5.8$  nm. In fact, such a stiffening effect was previously demonstrated for polymer films supported by a rigid substrate through AFM nanoindentation;<sup>7</sup> however, the widely held explanation of substrate effects fails to account for the findings here because the films are freestanding. Recently, similar stiffening behavior has also been observed in freestanding polystyrene (PS) films. In this case, the proposed mechanism lies in the formation of a mechanically confined interphase between the AFM tip and polymer under contact loading.<sup>47</sup> If this is true, altering the interfacial contact area should make a significant difference in the mechanical response. However, herein, the moduli measured by AFM tips with different radii (20 vs 100 nm) exhibit comparable values (Figure S7), thereby invalidating the contact-induced stiffening mechanism. This can be further exemplified by the nanobubble inflation test reporting the stiffening of the glassy compliance for ultrathin PS films even without the tip–polymer contact loading.<sup>48</sup> More reasonably, the overall mechanical response is supposed to come from not only the local area under the tip but also regions away from the contact. Besides, McKenna et al. argued that the surface tension acting on freestanding polymer films remained constant across thicknesses and failed to fully account for the stiffening.<sup>49</sup> Note that the annealing time was reported to have an influence on the mechanical properties of polymer films<sup>47</sup> in terms of residual stress induced by thermal annealing due to the mismatch in coefficients of thermal expansion between the film and substrate.<sup>50</sup> However, we expect that the freestanding

PMMA film suffers from a negligible thermal stress as it is suspended over the holes without contact with the substrate. Furthermore, the residual stress was found to drop considerably for ultrathin polymer films, possibly attributed to a higher molecular in-plane orientation that gives the lower thermal expansion coefficient and hence lower residual stress.<sup>50–52</sup> Here, we also performed the AFM deflection testing on the 10 nm PMMA film annealed for 24 h and found no difference in the measured modulus, demonstrating the full relaxation of polymer chains toward the equilibrium even with annealing for 2 h (Figure S8). Although there have been renewed concerns regarding whether annealing for 24 h is sufficient to reach equilibrium, we note that our procedure is comparable to the annealing protocol used in previous studies, where polymer films were annealed for 0.5–24 h.<sup>14,53,54</sup>

#### Molecular-Level Structure–Property Relationship.

Having excluded the abovementioned reasons for the mechanical stiffening of polymer ultrathin films, more attention was paid to two salient features in the thickness dependence of Young's moduli. First, as known, polymer chains typically take a random coil conformation with a radius of gyration ( $R_g$ ).<sup>55</sup> When the thickness decreases below  $2R_g$ , it was found that molecular chains would be distorted and subject to a contraction in the thickness direction while retaining the Gaussian conformation parallel to the surface.<sup>56</sup> Previous studies pointed out that the radius of gyration could be estimated based on molecular weight and takes the form  $R_g \cong 0.025 \sqrt{M_w}$  for PMMA.<sup>57</sup> According to the proposed empirical expression, the transition thickness here is approximated to be 35.2 nm, agreeing well with the transition region where the change of moduli occurs. The second feature gleaned from Figure 1d pertains to the maximum Young's modulus of 8.9 GPa approaching the purported single-chain modulus of PMMA ( $\sim$ 10 GPa).<sup>46</sup> More intriguingly, the corresponding thickness of 5.8 nm is consistent with the critical thickness ( $t_c$ ), defined by the segmental length ( $l$ ) and cross-sectional radius ( $r$ ) as  $t_c \cong 16r^2/l \approx 5.0$  nm,<sup>58–60</sup> below which the polymer

chains are elongated and oriented parallel to surfaces. Such a mechanical size effect is further confirmed for higher-molecular-weight ( $M_w \sim 1950$  K) PMMA, which shows a higher transition thickness at around  $2R_g$  of  $\sim 69.8$  nm and a maximum modulus of 10.1 GPa at  $t$  of  $\sim 6.4$  nm (Figure S12a). In this regard, a question of interest naturally arises as to whether the plausible structure–property relationship for PMMA films is coincidental or causal.

We first address this issue by characterizing polymer chain conformation with the small-angle X-ray scattering (SAXS) technique.<sup>56</sup> The intensity of X-rays was plotted as a function of the length of the scattering vector  $q$  in Figure 2a. It is evident that SAXS profiles for relatively thick films are highly overlapped, indicative of similar microstructural characteristics above the transition thickness, whereas the 11.2 nm thick film exhibits a distinct power law trend. To account for the scattering and gain more details in chain conformation, the SAXS intensity was assigned to three different contributions based on the Debye–Bueche approach<sup>61</sup>

$$I(q) = \frac{I_0}{1 + q^2\xi^2} + \frac{I_1}{(1 + q^2\zeta^2)^2} + I_{\text{background}} \quad (2)$$

The first component describes the scattering arising from the network structure of polymer chains with a Lorentzian feature, where  $\xi$  is the correlation length for density fluctuations.<sup>62</sup> The second component is referred to as the excess scattering from lateral correlations of the interface roughness between the polymer film and substrate. The parameter  $\zeta$  denotes the lateral correlation length of the roughness.<sup>56</sup> The additive term  $I_{\text{background}}$  is associated with the instrumental background scattering. As shown in Figure 2a, the model fits well with experimental curves over the range of  $0.146 < q < 1.015$  nm<sup>-1</sup>, and the corresponding fitting parameters are given in Figure 2b. Notably,  $\zeta$  shows comparable values for all three thicknesses, suggesting a similar contribution of interfacial roughness to the scattering. By contrast,  $\xi$  maintains almost the same value for thick films and increases below the transition thickness. Such an increased density fluctuation correlation length is associated with the reduced entanglement and increased excluded volume effects.<sup>62</sup> In addition, it also gives rise to the expansion of polymer chains and the ordering of the orientation of chains parallel to the surface. As a result, a stiffening of the chains is anticipated, and the single-chain stiffness is therefore expected to have an increased relevance to the mechanical performance of polymer films. Although the SAXS measurements were performed on supported films, the scattering from the interior of the film ( $\xi$ ) was separated from the substrate effect related to  $\zeta$  in the Debye–Bueche fitting, thus capable of capturing the chain conformation in free-standing films.

Note that it has been demonstrated in the literature, for instance by nanosphere sinking experiments, that some thin polymer films (e.g., polystyrene) show a decreasing  $T_g$  even down to room temperature due to a liquid-like surface layer under nanoconfinement.<sup>63–65</sup> To this end, we conducted temperature-dependent ellipsometric measurements of  $T_g$  for the freestanding PMMA films, which shows a  $T_g$  of  $\sim 89$  °C as the thickness decreases to 9.2 nm (Figure S11), agreeing well with the prediction by Roth et al.<sup>66</sup> Such an insignificant  $T_g$  reduction compared to the bulk  $T_g$  of 110 °C for PMMA has also been evidenced in the literature, where only a 10–30 °C reduction was reported for films as thin as 7 nm.<sup>67</sup> The slight

difference in the magnitude of  $T_g$  reduction is probably due to different annealing conditions and cooling rates in the sample preparation.<sup>68</sup> Despite few entanglements, the molecular chains are still in a glassy state since the modulus is increased by gigapascals.

To shed further light on the thickness dependence of chain structures, scanning near-field optical microscopy (SNOM) was adopted to obtain nanospectroscopic insight into the PMMA films. Combining infrared (IR) spectroscopy with scanning probe microscopy, SNOM allows chemical imaging with molecular-level spectroscopic specificity and an  $\sim 15$  nm lateral spatial resolution.<sup>69</sup> Figure 2c,2d presents the AFM topography image and corresponding SNOM image at 1730 cm<sup>-1</sup>, respectively. To circumvent the substrate effect on the spectral near-field response, sequential imaging at different wavelengths was performed on suspended regions and IR spectra were obtained, as shown in Figure 2e. Despite the existence of some impurity peaks possibly arising from the instrumental background, a 1  $\mu$ m thick PMMA film exhibits a broad peak at around 1730 cm<sup>-1</sup> attributed to the C=O stretching bond.<sup>70</sup> Its full width at half-maximum (FWHM) remains almost constant at around 20 cm<sup>-1</sup> as film thickness decreases to 66.4 nm while precipitously dropping to 13.6 cm<sup>-1</sup> for a thickness of 11.2 nm. In crystalline or semicrystalline polymers, narrower peaks are commonly associated with higher crystallinity.<sup>71</sup> Though the bulk atactic PMMA is amorphous, the peak narrowing may indicate a higher degree of order in nanoconfined films. The peak shows a slight blue shift for the 11.2 nm thick film, which is consistent with higher order within a denser packing of carbonyls.<sup>72,73</sup> We also conducted peak force infrared microscopic (PFIR) imaging, as shown in Figure 2f, which presents the same variation trend of the characteristic peak and confirms the observed microstructural evolution of PMMA chains upon decreasing thickness.<sup>74</sup> In contrast, for 1950 K PMMA films, such a peak shift and narrowing can be observed even at a thickness of  $\sim 62$  nm, implying a higher transition thickness due to the higher molecular weight as evidenced by the mechanical measurements (Figure S12b).

**Theoretical Analysis of Mechanical Stiffening Mechanisms.** According to the structural characterization results, the observed stiffening behavior is correlated to the extended chains that are oriented parallel to surfaces under nanoconfinement. It is worth noting that such a transition in chain conformation can lead to transverse isotropy: the elastic constants remain the same in all directions within the plane but would be different from those in the thickness direction. However, for thin films, the elastic modulus measured by the AFM deflection test is the in-plane modulus, while the thickness direction modulus barely shows any effects on the mechanical response.<sup>75</sup> To gain a better understanding of such a size-dependent structure–property relationship, MD simulations were carried out to investigate the deformation behavior of PMMA systems. First, the root-mean-square end-to-end distance ( $R_{ee}$ ) was measured based on averaging over all molecules of the systems at the end of the relaxation process to quantitatively describe the three-dimensional (3D) chain conformation. Herein, the system is relaxed and then quenched to room temperature to achieve amorphous configurations. While the periodic and fixed boundary conditions were applied in in-plane and thickness directions, respectively, for confined 5 nm thin film systems prior to the thermal relaxation and quenching process, bulk algorithm without constraint in the

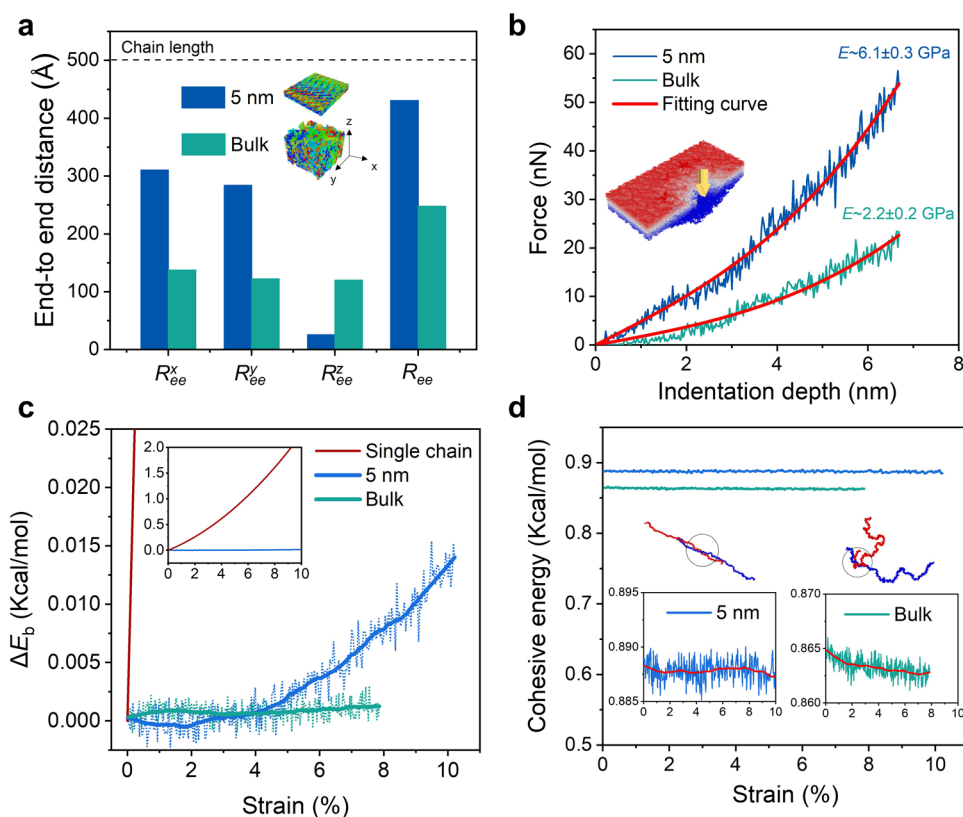


**Figure 3.** Molecular dynamics simulations. (a) Root-mean-square end-to-end distance of polymer chains in 3D ( $R_{ee}$ ) and components in three directions as indicated in the inset. (b) MD simulation results showing force-deflection curves and Young's modulus of PMMA bulk and 5 nm thin films. (c) Bond energy change ( $\Delta E_b$ ) as a function of strain for different PMMA systems. The dotted lines represent the raw data, with noises attributed to thermal vibrations in the systems, which are smoothed into solid lines to highlight the trend. The inset is the zoom-out for the same plot to more clearly show the single-chain curve. (d) Cohesive energy as a function of strain for PMMA bulk and 5 nm thin film. The insets are the zoom-in for the same plot to show the different trend upon increasing strain, corresponding to distinct chain entanglements for PMMA bulk and thin film.

thickness direction was used to create a 20 nm thick sample to represent the bulk polymer configuration. As shown in Figure 3a, the randomly coiled state of chains with highly entangled density can be seen for bulk PMMA. The consequent  $R_{ee}$  appears isotropic and shrinks to around 25 nm as compared with the chain length of  $\sim 50$  nm (equivalent to 200 repeating monomers). Note that, albeit shorter than the chain length in experiments (at the micron level), the longest computationally feasible chain length was adopted here to minimize the possible length effect on the results. As the thickness is reduced, appreciable changes in polymer chain packing can be anticipated. The film surfaces act as boundaries to restrict the free arrangement of the polymer chains so that the end-to-end distance component in the  $z$ -direction ( $R_{ee}^z$ ) is suppressed; however, the 3D  $R_{ee}$  displays an opposite trend and is measured to be 44.0 nm at a film thickness of 5 nm, approaching the chain length. This signifies an in-plane expansion of chains with  $R_{ee}^x$  and  $R_{ee}^y$  increasing from  $\sim 13.7$  nm and  $\sim 12.2$  to  $\sim 31.0$  nm and  $\sim 28.4$  nm, respectively, under nanoconfinement (Figure 3a), which is consistent with the aforementioned SAXS results. As the chain length in the experiment is much higher than that in simulations, the variation of  $R_{ee}$  upon the decreasing thickness is expected to be more significant. Young's moduli were obtained by fitting the computed force-deflection curves for PMMA systems under deflection loading based on eq 1, as illustrated in Figure 3b. An increasing modulus is observed as the film thickness decreases,

from the bulk value of 2.2 GPa to 6.1 GPa for the 5 nm thin film, in accordance with the stiffening behavior observed in experiments. Note that Young's modulus obtained in simulations is relatively lower than that in experimental observations, possibly due to the difference in the system size, which is associated with tip size, hole radius, and molecular chain length. The difference in chain length (nm vs  $\mu\text{m}$ ) may also be a potential reason for the softening behavior as reported in previous simulations, where the long chain length with a large in-plane simulation box dimensions used in this work provides relatively higher entanglements and reduced mobility of the chains, preventing chains from gaining the energetically favorable coiled shape. However, the overall trend and the magnitude of the mechanical enhancement, i.e., almost threefold increase in Young's modulus for 5 nm thin film compared to that in bulk, are observed for both the simulations and experiments.

It should be noted that the single-chain modulus is not constant across a wide range of strains. In particular, the simulations demonstrate that the stretching of a PMMA chain yields a nonlinear stress-strain curve that exhibits a two-stage feature (Figure S15), coinciding with conventional views that highlighted a combination of both entropic and enthalpic elasticities.<sup>76</sup> Generally, the former corresponds to the conformational transition at low extensions, wherein the chain behaves like a spring with a restoring force in entropic origin; the latter stems from the straining of backbones,

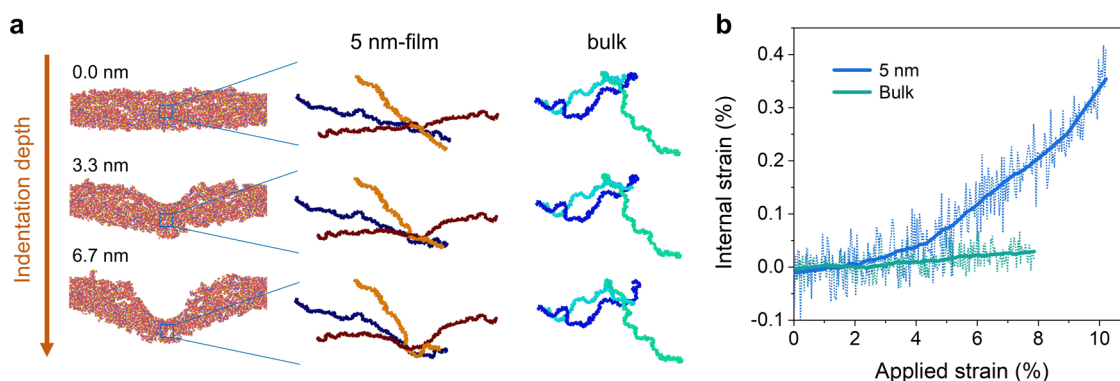


**Figure 4.** Entropic contribution to the chain stiffness. (a) Simulation snapshots of representative chains in 5 nm thin film and bulk, showing the chain deformation at different deflections under the tip. (b) Plot of the internal strain in backbones as a function of applied strain for 5 nm thin film and bulk PMMA.

inducing elongation and rotation of covalent bonds.<sup>76</sup> According to linear fitting of the stress–strain curve in two different stages (Figure S15), the chain stiffness was approximated to be 20.4 and 51.6 GPa for the entropic “spring” and backbone, respectively, yet both are higher than the reported value ( $\sim 10$  GPa) that was experimentally measured by the uniaxial tension of prestretched PMMA platelets. Therein, the softening mechanical response was possibly convoluted by the influence of intermolecular interactions and imperfect alignment.<sup>46</sup> Even so, it can be concluded that the mechanical property of the nanoconfined polymer film is on par with that of artificially aligned polymer structures, thanks to the chain stiffness effect. In fact, such a chain stiffness effect can be further validated by a molecular composite model,<sup>20</sup> where the load-bearing chains act as the reinforcing phase and are responsible for the mechanical stiffening (Figure S16).

Going one step further, it is necessary to ascertain the exact contributions of entropy and enthalpy in polymer networks and unveil their load-carrying characteristics during the deformation. We first look into the enthalpic resistance to stretching derived from the backbone rigidity. As depicted in Figure 3c, the averaged change in bond energy ( $\Delta E_b$ ) was examined to reflect the elongation of backbones. Herein,  $\Delta E_b$  is defined as  $\Delta E_b = (E_b(\epsilon) - E_b^0)/N_b$ , in which  $E_b(\epsilon)$  and  $E_b^0$  are the total bond energy at strained and unstrained states, respectively, and  $N_b$  is the number of bonds in both backbones and side groups. To compare the mechanical responses of PMMA films and single chains,  $\Delta E_b$  is plotted as a function of strain, which is converted from deflection based on the contact radius measurement and force-deflection curves, as shown in Figure S14. The obtained strain is localized under the tip and provides an overestimation of the overall strain given the inhomogeneous strain distribution in deflected PMMA systems; however, it would not lead to a change of the conclusion. Remarkably, bulk PMMA shows negligible variation in  $\Delta E_b$  within the whole loading range because the mechanical response of glassy polymer is dominated by the nonbonded interactions between the chains, rather than the tensile deformation of the chains themselves. By comparison, the greatly reduced entanglement density in thin films attenuates the contribution of intermolecular interactions, so that the cohesive energy varies little over the strain range (left inset in Figure 3d).<sup>18</sup> Notably, the cohesive energy of 5 nm thin film is slightly higher than that for bulk, possibly due to the local parallel orientation of neighboring chain segments

that provides stronger molecular interactions even for disentangled chains (left inset in Figure 3d). The unfolded and oriented chains in the confined geometry also facilitate the stretching along the loading direction so that the stressed C–C bonds in the backbone endow the system with a higher load-bearing capacity. Consequently, thin films exhibit an increasing tendency of  $\Delta E_b$  with applied strain, indicating an intensified enthalpic effect due to the backbone straining. The fluctuation in the initial plateau stage ( $< 2\%$  strain) is possibly attributed to the localized compression/bending deformation of PMMA chains under the tip, which should be suppressed by larger holes (compared to AFM tips) in experiments, allowing for the global stretching-dominated deformation of PMMA in the suspended region. Despite the contribution of backbone straining to Young’s modulus, the increase of  $\Delta E_b$  for thin films is still much below that of single chains (inset of Figure 3c). For instance, the  $\Delta E_b$  for 5 nm thin film is only  $\sim 0.5\%$  of that for single chain at 10% strain, suggesting that the covalent bonds are far from fully stretched and the enthalpic contribution may not be the dominant role in the elastic response.

To better understand the stiffening mechanism, we look into the chain deformation mechanism at the molecular level. Figure 4a gives the snapshots of representative chain configurations in both 5 nm thin film and bulk at different deflections under the tip during the deformation. In line with the discussion above, at zero strain, the geometrical confinement induces the chains to become unfolded and extended for thin films. The decreased configurational freedom results in higher entropic stiffness of chains, resembling stiff prestretched springs.<sup>77</sup> In addition, as the chains are disentangled, one might indicate that the entropic “spring” action is allowed to operate. As shown in Figure 4a, the increasing strain mainly results in the conformational transition of chains along the tip surface. Such a continuous chain elongation could cause further entropy reduction and generate a high entropic stress that contributes to the mechanical stiffening.<sup>77</sup> By comparison, the averaged internal strain in backbones is limited to 0.4% at the applied strain of 10% (Figure 4b), suggesting that the enthalpic effect is limited during the deformation. On the other hand, the chains in bulk PMMA appear curved and only subject to slight reorientation with negligible conformational change due to the physical constraint of entanglements. The backbone straining is also considerably suppressed, which confirms the load-bearing role of secondary bonds within entanglements rather than individual chains for bulk.

**Discussion.** The literature is replete with contradictory reports in the manifestation of size effect for nanoconfined polymer films. It would, therefore, be highly desirable to make a detailed comparison among various testing methods to gain an insight into the micromechanical mechanism. Note that polymers with similar backbone lengths but different conjugation or side chains can exhibit different entanglement densities and hence distinct mechanical performance.<sup>18,78</sup> Here, we focused on the mechanical measurements of PMMA films and normalized the film modulus ( $E^{\text{film}}$ ) by the bulk value ( $E^{\text{bulk}}$ ) for better visualization of the size-dependent transition.

As shown in Figure 5, bubble inflation measurements display an independence of thickness in the modulus of PMMA films,

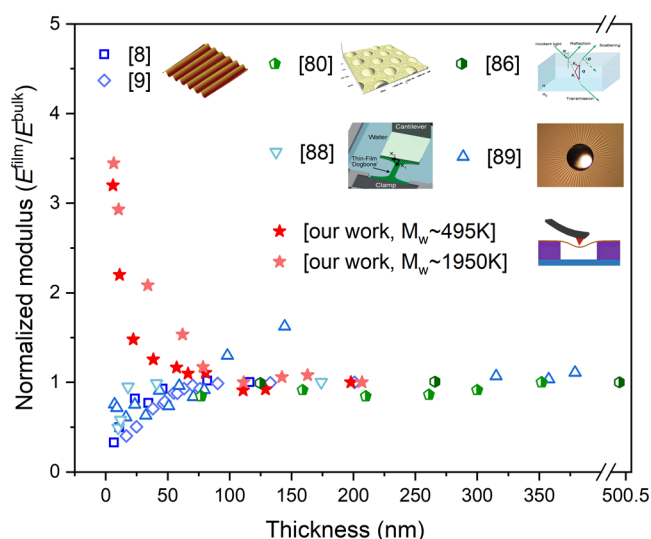


**Figure 5.** Comparison of the thickness dependence of normalized modulus ( $E^{\text{film}}/E^{\text{bulk}}$ ) for PMMA films measured by different testing methods, including surface wrinkling, bubble inflation, Brillouin light scattering, uniaxial stretching, capillary wrinkling, and AFM deflection testing. The inset figures are reproduced with permission.<sup>8,9,80,86,88,89</sup>

likely due to the film thickness not being sufficiently low for the onset of a transition.<sup>79</sup> In reality, unusual rubbery stiffening behaviors have been revealed by the bubble inflation for a variety of polymer thin films.<sup>51,53,80</sup> To explain the rubbery stiffening results, Ngai et al. proposed a coupling model from the viewpoint of the macroscopic polymer viscoelasticity.<sup>81,82</sup> Specifically, they indicated that the strength of rubbery stiffening was related to the extent of the separation of the segmental  $\alpha$  relaxation and the Rouse modes through the segmental coupling parameter. Later, such a coupling model was validated by McKenna's group through the linear correlation between the rubbery stiffening index, dynamic fragility index, and coupling parameter.<sup>51,53</sup> However, as the segmental  $\alpha$  relaxation and Rouse modes are associated with transition to the rubbery plateau, the coupling model cannot be used to account for the glassy stiffening observed for PS and polycarbonate (PC) films in nanobubble inflation experiments as well as for PMMA films in our work.<sup>48,83</sup> Therefore, we speculate that, analogous to AFM deflection testing, the enhanced modulus from nanobubble inflation results should not be related to the interactions between chain segments but rather more likely dominated by the stiffness of the polymer chains themselves. In this case, molecular chains act as the

load-bearing elements and are supposed to be more sensitive to the deformation modes. Particularly, the biaxial loading of the film would allow polymer chains to be purely stretched and hence highlight the chain stiffness contribution. Note that the molecular composite model prediction is found inconsistent with the rubbery stiffening results (e.g., poly(ethyl methacrylate)),<sup>53</sup> possibly because the interchain cooperativity and intermolecular interactions are neglected in the model; besides, the single-chain stiffness used in the composite model should be in entropic nature for the rubbery state, whereas the inclusion of backbone rigidity contribution may result in an overestimation of Young's modulus.

In striking contrast, the surface wrinkling method usually shows a descending trend of Young's moduli for PMMA films with decreasing thickness (hollow symbols in Figure 5).<sup>8,9</sup> It has been documented that polymer chains are prone to disentanglement with decreasing thickness, especially near the free surface, creating a liquid-like surface layer.<sup>84,85</sup> The consequently increased segmental mobility would moderate the strength of intermolecular forces and lead to the decreased modulus. However, the insignificant reduction of  $T_g$  for PMMA thin films here may suppress the effect of the liquid surface layer on the mechanical properties, which coincides with the strong molecular interactions for disentangled chains observed in MD simulations. In terms of the long relaxation time of PMMA ( $\sim 10^3$  s) at room temperature, the high strain rate ( $\sim 10^{-1}$  s $^{-1}$ ) in the AFM deflection testing is also reported to freeze the mobile chains; thus, even the enhanced mobility might not play a role in the mechanical response.<sup>12</sup> In addition, the interchain interaction-governed elasticity mechanism fails to interpret the widely observed—but not yet understood—discrepancy in the mechanical size effect of polymer films. Torres et al. have recently pointed out that the wrinkling measurements actually probe the elastic response through the thickness of polymer films.<sup>78</sup> One potential reason for the softening behavior would hence be that the applied stress is not aligned with chain orientation direction, coinciding with the molecular mechanism proposed in our work. As discussed above, individual chains instead of intermolecular interactions may play a significant role in the mechanical response under nanoconfinement, so that the measured moduli would be influenced by stress states of polymer chains. The fact is that the wrinkling loading may apply compression or bending deformation to the chains, thus negating the chain stiffness effect in terms of the flexibility of chains. Interestingly, a recent study by Page et al. reported a stiffening behavior of ultrathin Nafion films based on surface wrinkling method, which was also interpreted by the chain stiffness effect.<sup>20</sup> This might be, on the one hand, attributed to the semicrystalline nature of poly(tetrafluoroethylene) (PTFE) backbones. Highly ordered domains where the molecular chains are densely packed would respond collectively to the external load and behave more resistant to compression/bending load deformation. It is hence not surprising that the chain stiffness plays a role in the crystalline structure and contributes to the mechanical stiffening. On the other hand, it has been demonstrated that not all polymers examined by surface buckling exhibit a decrease in modulus for their thin films, depending on the polymer flexibility.<sup>78</sup> In the amorphous phase of Nafion, the presence of bulky side chains and pendant ionic groups on PTFE backbones may change the chain flexibility and conformation, thus giving rise to a distinct thickness dependence of modulus from that of PMMA and PS.



Similarly, the stresses of polymer chains are largely compression-dominated in substrate-supported nanoindentation. This accounts for the softening of supported polymer films when the substrate effect was excluded in simulations.<sup>26</sup> Even the stress response of the rigid substrate is separated, the compression state is maintained for polymer chains. By contrast, in an earlier experiment by Fytas et al.,<sup>86</sup> Young's modulus was found to be constant for PMMA films within the range of 124–490 nm (Figure 5), as inferred from the measured speed of phonons in the films. This can be explained by the zero-strain state of polymer chains in the Brillouin light scattering (BLS) measurements.<sup>87</sup> More recently, a water-supported uniaxial tensile test has also been exploited to measure the mechanics of ultrathin PMMA films, and the elastic modulus is found to decrease when the thickness reduces to below 20 nm, as shown in Figure 5.<sup>88</sup> The discrepancy might be explicable by different responses of long-range and local chain dynamics to the nanoconfinement.<sup>13</sup> While all of the chains within the micron-sized holes are subject to pure stretching in the AFM deflection and bubble inflation, they would suffer from complex stress states during large-scale in-plane tensile deformation, especially considering the presence of surface crumples and Poisson's effect. Furthermore, the water absorption or diffusion in the polymer film is deemed as primary factors for the softening mechanism.<sup>88</sup> The presence of water may also influence the mechanical response of polymer thin films floating on water, where capillary wrinkling patterns are formed upon the addition of a water droplet onto the film center. The modulus is estimated to be almost constant for PMMA films as thin as 7 nm (Figure 5), possibly related to the effective entanglement molecular weight due to confinement.<sup>89</sup> We should also note that the estimation of modulus based on wrinkling method heavily relies on the theoretical model that assumes that the bending rigidity ( $D$ ) of an elastic plate is related to its thickness ( $t$ ) and the elastic moduli ( $E$ ) of the material by  $D \sim Et^3$ .<sup>90</sup> Nevertheless, it is an open question whether the classic  $D \sim E$  relation holds well for ultrathin polymer films with more disentangled chains. If we consider a softening compression/bending response of an individual chain, we may expect  $D < Et^3$  for ultrathin amorphous polymer films, which means the theoretical prediction gives an underestimation of the modulus for ultrathin polymer films. All in all, the single-chain-dominated deformation mechanism tends to give a unified explanation for distinct thickness-dependent behaviors of nanoconfined polymer films in the framework of mechanical concepts.

## CONCLUSIONS

This work provided a combined experimental and computational study on the elastic properties of glassy polymer films with thickness on the order of individual polymer chains. AFM deflection testing revealed a pronounced increase in Young's modulus for freestanding PMMA films with decreasing thickness. Such a mechanical stiffening was ascribed to a transition in chain conformation under nanoconfinement. Both the SAXS and SNOM results demonstrated that molecular chains tended to be disentangled, extended, and oriented parallel to the film surface once the thickness was below the characteristic length ( $2R_g$ ). Consequently, these chains play a more dominant role in load bearing over the vdW interactions in entanglements, as evidenced by MD modeling. Specifically, although backbone straining was enabled due to the enhanced

interchain coupling in the confined geometry, the enthalpic contribution to the chain stiffness was found to be suppressed in terms of the limited change of bond energy. The decomposition of strain and chain configuration analysis instead highlighted the more significant contribution of entropic effects on the mechanical stiffening as the conformational transition dominated the deformation of chains. The entropy reduction gives rise to a high entropic stress and therefore accounts for the dominant contribution for the stiffening mechanism.

Our results advance the fundamental understanding of the deformation mechanisms in nanoconfined polymer films and elucidate the competing contributions to the mechanical nanoscale size effect between single chains and entanglements. The proposed mechanism offers a viable resolution to contrasting observations, attributing the film softening to compressed/bent chains, which is uncondusive to the chain stiffness effect. With the nanoconfinement as a prerequisite, biaxial stretching is deemed effective to trigger the chain stiffness effect. In addition to the scientific fundamentals, the thorough insight into these nanoconfinement paradigms is also of technological importance in view of the vast range of applications of polymer nanostructures. The presented molecular origins of this size effect enable us with an opportunity to tune the length scale that the chain stiffness effect activates, through the rationalized optimization of local conformations and chemical structures (e.g., backbone and side groups). The exploitation of such design principles may pave a pathway for tailored mechanical properties of functional nanodevices and nanocomposites, where even thinner and stiffer layers are desired.

## ASSOCIATED CONTENT

### Supporting Information

The Supporting Information is available free of charge at <https://pubs.acs.org/doi/10.1021/acs.macromol.1c02270>.

Preparation and characterization of freestanding PMMA films; atomic force microscopy (AFM) deflection test; structural characterization; molecular dynamics (MD) simulation; and molecular composite model (PDF)

## AUTHOR INFORMATION

### Corresponding Authors

Gilbert C. Walker – Department of Chemistry, University of Toronto, Toronto, Ontario M5S 3H6, Canada;

[orcid.org/0000-0002-5248-5498](https://orcid.org/0000-0002-5248-5498);

Email: [gilbert.walker@utoronto.ca](mailto:gilbert.walker@utoronto.ca)

Chandra Veer Singh – Department of Materials Science and Engineering, University of Toronto, Toronto, Ontario M5S 3E4, Canada; [orcid.org/0000-0002-6644-0178](https://orcid.org/0000-0002-6644-0178);

Email: [chandraveer.singh@utoronto.ca](mailto:chandraveer.singh@utoronto.ca)

Tobin Filleter – Department of Mechanical and Industrial Engineering, University of Toronto, Toronto, Ontario M5S 3G8, Canada; [orcid.org/0000-0003-2609-4773](https://orcid.org/0000-0003-2609-4773);

Email: [filleter@mie.utoronto.ca](mailto:filleter@mie.utoronto.ca)

### Authors

Guorui Wang – Department of Mechanical and Industrial Engineering, University of Toronto, Toronto, Ontario M5S 3G8, Canada; [orcid.org/0000-0002-1746-3410](https://orcid.org/0000-0002-1746-3410)

Farzin Najafi – Department of Mechanical and Industrial Engineering, University of Toronto, Toronto, Ontario M5S 3G8, Canada

Kevin Ho – Department of Chemistry, University of Toronto, Toronto, Ontario M5S 3H6, Canada; [orcid.org/0000-0003-2688-2606](https://orcid.org/0000-0003-2688-2606)

Mahdi Hamidinejad – Department of Mechanical and Industrial Engineering, University of Toronto, Toronto, Ontario M5S 3G8, Canada; [orcid.org/0000-0003-3137-1990](https://orcid.org/0000-0003-3137-1990)

Teng Cui – Department of Mechanical and Industrial Engineering, University of Toronto, Toronto, Ontario M5S 3G8, Canada; [orcid.org/0000-0002-3218-2721](https://orcid.org/0000-0002-3218-2721)

Complete contact information is available at:

<https://pubs.acs.org/10.1021/acs.macromol.1c02270>

## Author Contributions

<sup>||</sup>G.W. and F.N. contributed equally to this work.

## Notes

The authors declare no competing financial interest.

## ACKNOWLEDGMENTS

The authors acknowledge financial support from the Natural Sciences and Engineering Research Council of Canada (NSERC), the Canada Foundation for Innovation (CFI), the Erwin Edward Hart Professorship, the Ontario Ministry of Research and Innovation Early Career Researcher Award, the Canada Research Chairs Program, and the Ontario Research Funds—Research Excellence programme. MD simulations were performed at the SciNet and Calculquebec consortia. SciNet is funded by the Canada Foundation for Innovation under the auspices of Compute Canada, the Government of Ontario, Ontario Research Fund-Research Excellence, and the University of Toronto. SAXS measurements were performed at The Structural & Biophysical Core (SBC) Facility with technical assistance from Greg Wasney.

## REFERENCES

- (1) Xu, J.; Wang, S. H.; Wang, G. J. N.; Zhu, C. X.; Luo, S. C.; Jin, L. H.; Gu, X. D.; Chen, S. C.; Feig, V. R.; To, J. W. F.; Rondeau-Gagne, S.; Park, J.; Schroeder, B. C.; Lu, C.; Oh, J. Y.; Wang, Y. M.; Kim, Y. H.; Yan, H.; Sinclair, R.; Zhou, D. S.; Xue, G.; Murmann, B.; Linder, C.; Cai, W.; Tok, J. B. H.; Chung, J. W.; Bao, Z. N. Highly Stretchable Polymer Semiconductor Films through the Nanoconfinement Effect. *Science* **2017**, *355*, 59–64.
- (2) Podsiadlo, P.; Kaushik, A. K.; Arruda, E. M.; Waas, A. M.; Shim, B. S.; Xu, J.; Nandivada, H.; Pumplun, B. G.; Lahann, J.; Ramamoorthy, A.; Kotov, N. A. Ultrastrong and Stiff Layered Polymer Nanocomposites. *Science* **2007**, *318*, 80–83.
- (3) Oh, J. Y.; Son, D.; Katsumata, T.; Lee, Y.; Kim, Y.; Lopez, J.; Wu, H. C.; Kang, J.; Park, J.; Gu, X.; Mun, J.; Wang, N. G.; Yin, Y.; Cai, W.; Yun, Y.; Tok, J. B.; Bao, Z. Stretchable Self-Healable Semiconducting Polymer Film for Active-Matrix Strain-Sensing Array. *Sci. Adv.* **2019**, *5*, No. eaav3097.
- (4) Zhu, T. T.; Bushby, A. J.; Dunstan, D. J. Materials Mechanical Size Effects: A Review. *Mater. Technol.* **2008**, *23*, 193–209.
- (5) Uchic, M. D.; Dimiduk, D. M.; Florando, J. N.; Nix, W. D. Sample Dimensions Influence Strength and Crystal Plasticity. *Science* **2004**, *305*, 986–989.
- (6) Xia, W.; Song, J.; Hsu, D. D.; Keten, S. Understanding the Interfacial Mechanical Response of Nanoscale Polymer Thin Films Via Nanoindentation. *Macromolecules* **2016**, *49*, 3810–3817.
- (7) Tweedie, C. A.; Constantinides, G.; Lehman, K. E.; Brill, D. J.; Blackman, G. S.; Van Vliet, K. J. Enhanced Stiffness of Amorphous

Polymer Surfaces under Confinement of Localized Contact Loads. *Adv. Mater.* **2007**, *19*, 2540–2546.

(8) Stafford, C. M.; Vogt, B. D.; Christopher, H.; Duangrut, J.; Rui, H. Elastic Moduli of Ultrathin Amorphous Polymer Films. *Macromolecules* **2006**, *39*, 5095–5099.

(9) Torres, J. M.; Stafford, C. M.; Vogt, B. D. Manipulation of the Elastic Modulus of Polymers at the Nanoscale: Influence of Uv-Ozone Cross-Linking and Plasticizer. *ACS Nano* **2010**, *4*, 5357–5365.

(10) Xia, W.; Keten, S. Size-Dependent Mechanical Behavior of Free-Standing Glassy Polymer Thin Films. *J. Mater. Res.* **2015**, *30*, 36–45.

(11) Xia, W.; Keten, S. Interfacial Stiffening of Polymer Thin Films under Nanoconfinement. *Extreme Mech. Lett.* **2015**, *4*, 89–95.

(12) Yiu, P. M.; Yuan, H.; Gu, Q.; Gao, P.; Tsui, O. K. C. Strain Rate and Thickness Dependences of Elastic Modulus of Free-Standing Polymer Nanometer Films. *ACS Macro Lett.* **2020**, *9*, 1521–1526.

(13) Galuska, L. A.; Muckley, E. S.; Cao, Z.; Ehlenberg, D. F.; Qian, Z.; Zhang, S.; Rondeau-Gagne, S.; Phan, M. D.; Ankner, J. F.; Ivanov, I. N.; Gu, X. Smart Transfer Method to Directly Compare the Mechanical Response of Water-Supported and Free-Standing Ultrathin Polymeric Films. *Nat. Commun.* **2021**, *12*, No. 2347.

(14) Bay, R. K.; Crosby, A. J. Uniaxial Extension of Ultrathin Freestanding Polymer Films. *ACS Macro Lett.* **2019**, *8*, 1080–1085.

(15) Meijer, H. E. H.; Govaert, L. E. Mechanical Performance of Polymer Systems: The Relation between Structure and Properties. *Prog. Polym. Sci.* **2005**, *30*, 915–938.

(16) Young, R. J. Polymer Glasses, Mechanical Properties Of: Yielding. In *Encyclopedia of Materials – Science and Technology*; Buschow, K. H. J., Ed.; Elsevier: New York, 2001; Vol. 1, pp 7330–7340.

(17) Si, L.; Massa, M. V.; Dalnoki-Veress, K.; Brown, H. R.; Jones, R. A. Chain Entanglement in Thin Freestanding Polymer Films. *Phys. Rev. Lett.* **2005**, *94*, No. 127801.

(18) Sussman, D. M.; Tung, W.-S.; Winey, K. I.; Schweizer, K. S.; Riggleman, R. A. Entanglement Reduction and Anisotropic Chain and Primitive Path Conformations in Polymer Melts under Thin Film and Cylindrical Confinement. *Macromolecules* **2014**, *47*, 6462–6472.

(19) Isaacson, S. G.; Lioni, K.; Volksen, W.; Magbitang, T. P.; Matsuda, Y.; Dauskardt, R. H.; Dubois, G. Fundamental Limits of Material Toughening in Molecularly Confined Polymers. *Nat. Mater.* **2016**, *15*, 294–298.

(20) Page, K. A.; Kusoglu, A.; Stafford, C. M.; Kim, S.; Kline, R. J.; Weber, A. Z. Confinement-Driven Increase in Ionomer Thin-Film Modulus. *Nano Lett.* **2014**, *14*, 2299–2304.

(21) Bemis, J. E.; Akhremitchev, B. B.; Walker, G. C. Single Polymer Chain Elongation by Atomic Force Microscopy. *Langmuir* **1999**, *15*, 2799–2805.

(22) Akhremitchev, B. B.; Walker, G. C. Effect of Finite Sample Thickness on Elasticity Determination Using Atomic Force Microscopy. *Langmuir* **1999**, *15*, 5630–5634.

(23) Chiodini, S.; Ruiz-Rincon, S.; Garcia, P. D.; Martin, S.; Kettelhoit, K.; Armenia, I.; Werz, D. B.; Cea, P. Bottom Effect in Atomic Force Microscopy Nanomechanics. *Small* **2020**, *16*, No. e2000269.

(24) Chung, P. C.; Glynos, E.; Green, P. F. The Elastic Mechanical Response of Supported Thin Polymer Films. *Langmuir* **2014**, *30*, 15200–15205.

(25) Oommen, B.; Van Vliet, K. J. Effects of Nanoscale Thickness and Elastic Nonlinearity on Measured Mechanical Properties of Polymeric Films. *Thin Solid Films* **2006**, *513*, 235–242.

(26) Li, L.; Encarnacao, L. M.; Brown, K. A. Polymer Nanomechanics: Separating the Size Effect from the Substrate Effect in Nanoindentation. *Appl. Phys. Lett.* **2017**, *110*, No. 043105.

(27) Hsu, D. D.; Xia, W.; Song, J.; Keten, S. Glass-Transition and Side-Chain Dynamics in Thin Films: Explaining Dissimilar Free Surface Effects for Polystyrene Vs Poly(Methyl Methacrylate). *ACS Macro Lett.* **2016**, *5*, 481–486.

- (28) Wang, G.; Dai, Z.; Liu, L.; Hu, H.; Dai, Q.; Zhang, Z. Tuning the Interfacial Mechanical Behaviors of Monolayer Graphene/Pmma Nanocomposites. *ACS Appl. Mater. Interfaces* **2016**, *8*, 22554–22562.
- (29) Sader, J. E.; Chon, J. W. M.; Mulvaney, P. Calibration of Rectangular Atomic Force Microscope Cantilevers. *Rev. Sci. Instrum.* **1999**, *70*, 3967–3969.
- (30) Cao, C.; Mukherjee, S.; Liu, J.; Wang, B.; Amirmaleki, M.; Lu, Z.; Howe, J. Y.; Perovic, D.; Sun, X.; Singh, C. V.; Sun, Y.; Filleter, T. Role of Graphene in Enhancing the Mechanical Properties of Tio<sub>2</sub>/Graphene Heterostructures. *Nanoscale* **2017**, *9*, 11678–11684.
- (31) Ho, K.; Kim, K. S.; Gilburd, L.; Mirzoyan, R.; de Beer, S.; Walker, G. C. Nanoscale Subsurface Morphologies in Block Copolymer Thin Films Revealed by Combined near-Field Infrared Microscopy and Mechanical Mapping. *ACS Appl. Polym. Mater.* **2019**, *1*, 933–938.
- (32) Torres, J. A.; Nealey, P. F.; de Pablo, J. J. Molecular Simulation of Ultrathin Polymeric Films near the Glass Transition. *Phys. Rev. Lett.* **2000**, *85*, 3221–3224.
- (33) Xia, W.; Lan, T. Interfacial Dynamics Governs the Mechanical Properties of Glassy Polymer Thin Films. *Macromolecules* **2019**, *52*, 6547–6554.
- (34) Mayo, S. L.; Olafson, B. D.; Goddard, W. A. Dreiding: A Generic Force Field for Molecular Simulations. *J. Phys. Chem. A* **1990**, *94*, 8897–8909.
- (35) Skountzos, E. N.; Anastassiou, A.; Mavrantzas, V. G.; Theodorou, D. N. Determination of the Mechanical Properties of a Poly (Methyl Methacrylate) Nanocomposite with Functionalized Graphene Sheets through Detailed Atomistic Simulations. *Macromolecules* **2014**, *47*, 8072–8088.
- (36) Plimpton, S. Fast Parallel Algorithms for Short-Range Molecular-Dynamics. *J. Comput. Phys.* **1995**, *117*, 1–19.
- (37) Stukowski, A. Visualization and Analysis of Atomistic Simulation Data with Ovito—the Open Visualization Tool. *Model. Simul. Mater. Sci. Eng.* **2009**, *18*, No. 015012.
- (38) Mark, J. E. *Physical Properties of Polymers Handbook*; Springer, 2007; Vol. 1076.
- (39) Xia, W.; Hsu, D. D.; Keten, S. Molecular Weight Effects on the Glass Transition and Confinement Behavior of Polymer Thin Films. *Macromol. Rapid Commun.* **2015**, *36*, 1422–1427.
- (40) Cao, G.; Gao, H. Mechanical Properties Characterization of Two-Dimensional Materials Via Nanoindentation Experiments. *Prog. Mater. Sci.* **2019**, *103*, 558–595.
- (41) Greaves, G. N.; Greer, A. L.; Lakes, R. S.; Rouxel, T. Poisson's Ratio and Modern Materials. *Nat. Mater.* **2011**, *10*, 823–837.
- (42) Shavit, A.; Riggleman, R. A. Influence of Backbone Rigidity on Nanoscale Confinement Effects in Model Glass-Forming Polymers. *Macromolecules* **2013**, *46*, 5044–5052.
- (43) Vella, D.; Davidovitch, B. Indentation Metrology of Clamped, Ultra-Thin Elastic Sheets. *Soft Matter* **2017**, *13*, 2264–2278.
- (44) Wunderlich, W. Physical Constants of Poly (Methyl Methacrylate). In *Polymer Handbook*; John Wiley & Sons, 1989; Vol. 78.
- (45) Ishiyama, C.; Higo, Y. Effects of Humidity on Young's Modulus in Poly (Methyl Methacrylate). *J. Polym. Sci., Part B: Polym. Phys.* **2002**, *40*, 460–465.
- (46) Urbanek, S.; Tashiro, K.; Kitayama, T.; Hatada, K. Crystallite Modulus of Double-Stranded Helices of Isotactic Poly-(Methylmethacrylate): The X-Ray Measurement and the Theoretical Calculation. *Polymer* **1999**, *40*, 3345–3351.
- (47) Liu, H.; Liu, W.; Fujie, T.; Nakajima, K. Contact-Induced Stiffening in Ultrathin Amorphous Polystyrene Films. *Polymer* **2018**, *153*, 521–528.
- (48) O'Connell, P. A.; Hutcheson, S. A.; McKenna, G. B. Creep Behavior of Ultra-Thin Polymer Films. *J. Polym. Sci., Part B: Polym. Phys.* **2008**, *46*, 1952–1965.
- (49) Xu, S.; O'Connell, P. A.; McKenna, G. B. Unusual Elastic Behavior of Ultrathin Polymer Films: Confinement-Induced/Molecular Stiffening and Surface Tension Effects. *J. Chem. Phys.* **2010**, *132*, No. 184902.
- (50) Chung, J. Y.; Chastek, T. Q.; Fasolka, M. J.; Ro, H. W.; Stafford, C. M. Quantifying Residual Stress in Nanoscale Thin Polymer Films Via Surface Wrinkling. *ACS Nano* **2009**, *3*, 844–852.
- (51) Yoon, H.; McKenna, G. B. "Rubbery Stiffening" and Rupture Behavior of Freely Standing Nanometric Thin Pib Films. *Macromolecules* **2017**, *50*, 9821–9830.
- (52) Ree, M.; Chu, C. W.; Goldberg, M. J. Influences of Chain Rigidity, in-Plane Orientation, and Thickness on Residual Stress of Polymer Films. *J. Appl. Phys.* **1994**, *75*, 1410–1419.
- (53) Li, X.; McKenna, G. B. Ultrathin Polymer Films: Rubbery Stiffening, Fragility, and Tg Reduction. *Macromolecules* **2015**, *48*, 6329–6336.
- (54) Torres, J. M.; Stafford, C. M.; Vogt, B. D. Elastic Modulus of Amorphous Polymer Thin Films: Relationship to the Glass Transition Temperature. *ACS Nano* **2009**, *3*, 2677–2685.
- (55) Kraus, J.; Muller-Buschbaum, P.; Kuhlmann, T.; Schubert, D. W.; Stamm, M. Confinement Effects on the Chain Conformation in Thin Polymer Films. *Europhys. Lett.* **2000**, *49*, 210–216.
- (56) Jones, R. L.; Kumar, K. S.; Ho, D. L.; Briber, R. M.; Russel, T. P. Chain Conformation in Ultrathin Polymer Films. *Nature* **1999**, *400*, 146–149.
- (57) O'Reilly, J. M.; Teegarden, D. M.; Wignall, G. D. Small- and Intermediate-Angle Neutron Scattering from Stereoregular Poly-(Methyl Methacrylate). *Macromolecules* **1985**, *18*, 2747–2752.
- (58) Boyer, R. F.; Miller, R. L. Polymer Chain Stiffness Parameter,  $\Sigma$ , and Cross-Sectional Area Per Chain. *Macromolecules* **1977**, *10*, 1167–1169.
- (59) Shuto, K.; Oishi, Y.; Kajiyama, T.; Han, C. C. Aggregation Structure of Two-Dimensional Ultrathin Polystyrene Film Prepared by the Water Casting Method. *Macromolecules* **1993**, *26*, 6589–6594.
- (60) Haley, J. C.; Lodge, T. P. Dynamics of a Poly(Ethylene Oxide) Tracer in a Poly(Methyl Methacrylate) Matrix: Remarkable Decoupling of Local and Global Motions. *J. Chem. Phys.* **2005**, *122*, No. 234914.
- (61) Pizzorusso, G.; Fratini, E.; Eiblmeier, J.; Giorgi, R.; Chelazzi, D.; Chevalier, A.; Baglioni, P. Physicochemical Characterization of Acrylamide/Bisacrylamide Hydrogels and Their Application for the Conservation of Easel Paintings. *Langmuir* **2012**, *28*, 3952–61.
- (62) Mukhopadhyay, M. K.; Jiao, X.; Lurio, L. B.; Jiang, Z.; Stark, J.; Sprung, M.; Narayanan, S.; Sandy, A. R.; Sinha, S. K. Thickness Induced Structural Changes in Polystyrene Films. *Phys. Rev. Lett.* **2008**, *101*, No. 115501.
- (63) Hutcheson, S. A.; McKenna, G. B. Nanosphere Embedding into Polymer Surfaces: A Viscoelastic Contact Mechanics Analysis. *Phys. Rev. Lett.* **2005**, *94*, No. 076103.
- (64) Paeng, K.; Swallen, S. F.; Ediger, M. D. Direct Measurement of Molecular Motion in Freestanding Polystyrene Thin Films. *J. Am. Chem. Soc.* **2011**, *133*, 8444–8447.
- (65) Sasaki, T.; Shimizu, A.; Mourey, T. H.; Thurau, C. T.; Ediger, M. D. Glass Transition of Small Polystyrene Spheres in Aqueous Suspensions. *J. Chem. Phys.* **2003**, *119*, 8730–8735.
- (66) Roth, C. B.; Pound, A.; Kamp, S. W.; Murray, C. A.; Dutcher, J. R. Molecular-Weight Dependence of the Glass Transition Temperature of Freely-Standing Poly(Methyl Methacrylate) Films. *Eur. Phys. J. E* **2006**, *20*, 441–448.
- (67) Sharp, J. S.; Forrest, J. A. Thickness Dependence of the Dynamics in Thin Films of Isotactic Poly (Methylmethacrylate). *Eur. Phys. J. E* **2003**, *12*, 97–101.
- (68) Fakhraai, Z.; Forrest, J. A. Probing Slow Dynamics in Supported Thin Polymer Films. *Phys. Rev. Lett.* **2005**, *95*, No. 025701.
- (69) Muller, E. A.; Pollard, B.; Raschke, M. B. Infrared Chemical Nano-Imaging: Accessing Structure, Coupling, and Dynamics on Molecular Length Scales. *J. Phys. Chem. Lett.* **2015**, *6*, 1275–1284.
- (70) Mastel, S.; Govyadinov, A. A.; de Oliveira, T. V. A. G.; Amenabar, I.; Hillenbrand, R. Nanoscale-Resolved Chemical Identification of Thin Organic Films Using Infrared near-Field Spectroscopy and Standard Fourier Transform Infrared References. *Appl. Phys. Lett.* **2015**, *106*, No. 023113.

(71) Hagemann, H.; Snyder, R. G.; Peacock, A. J.; Mandelkern, L. Quantitative Infrared Methods for the Measurement of Crystallinity and Its Temperature Dependence: Polyethylene. *Macromolecules* **1989**, *22*, 3600–3606.

(72) Dybal, J.; Spevacek, J.; Schneider, B. Ordered Structures of Syndiotactic Poly(Methyl Methacrylates) Studied by a Combination of Infrared, Raman, and Nmr-Spectroscopy. *J. Polym. Sci., Part B: Polym. Phys.* **1986**, *24*, 657–674.

(73) Pollard, B.; Muller, E. A.; Hinrichs, K.; Raschke, M. B. Vibrational Nano-Spectroscopic Imaging Correlating Structure with Intermolecular Coupling and Dynamics. *Nat. Commun.* **2014**, *5*, No. 3587.

(74) Wang, L.; Wang, H.; Wagner, M.; Yan, Y.; Jakob, D. S.; Xu, X. G. Nanoscale Simultaneous Chemical and Mechanical Imaging Via Peak Force Infrared Microscopy. *Sci. Adv.* **2017**, *3*, No. e1700255.

(75) Lee, C.; Wei, X.; Kysar, J. W.; Hone, J. Measurement of the Elastic Properties and Intrinsic Strength of Monolayer Graphene. *Science* **2008**, *321*, 385–388.

(76) Ortiz, C.; Hadziioannou, G. Entropic Elasticity of Single Polymer Chains of Poly(Methacrylic Acid) Measured by Atomic Force Microscopy. *Macromolecules* **1999**, *32*, 780–787.

(77) Alcoutlabi, M.; McKenna, G. B. Effects of Confinement on Material Behaviour at the Nanometre Size Scale. *J. Phys.: Condens. Matter* **2005**, *17*, R461–R524.

(78) Torres, J. M.; Wang, C.; Coughlin, E. B.; Bishop, J. P.; Register, R. A.; Riggleman, R. A.; Stafford, C. M.; Vogt, B. D. Influence of Chain Stiffness on Thermal and Mechanical Properties of Polymer Thin Films. *Macromolecules* **2011**, *44*, 9040–9045.

(79) Huang, C. K.; Lou, W. M.; Tsai, C. J.; Wu, T.-C.; Lin, H.-Y. Mechanical Properties of Polymer Thin Film Measured by the Bulge Test. *Thin Solid Films* **2007**, *515*, 7222–7226.

(80) O'Connell, P. A.; McKenna, G. B. Dramatic Stiffening of Ultrathin Polymer Films in the Rubbery Regime. *Eur. Phys. J. E* **2006**, *20*, 143–150.

(81) Ngai, K. L.; Prevosto, D.; Grassia, L. Viscoelasticity of Nanobubble-Inflated Ultrathin Polymer Films: Justification by the Coupling Model. *J. Polym. Sci., Part B: Polym. Phys.* **2013**, *51*, 214–224.

(82) Ngai, K. L.; Prevosto, D.; Capaccioli, S. A Perspective on Experimental Findings and Theoretical Explanations of Novel Dynamics at Free Surface and in Freestanding Thin Films of Polystyrene. *Philos. Mag.* **2016**, *96*, 854–869.

(83) O'Connell, P. A.; Wang, J.; Ishola, T. A.; McKenna, G. B. Exceptional Property Changes in Ultrathin Films of Polycarbonate: Glass Temperature, Rubbery Stiffening, and Flow. *Macromolecules* **2012**, *45*, 2453–2459.

(84) Vogt, B. D. Mechanical and Viscoelastic Properties of Confined Amorphous Polymers. *J. Polym. Sci., Part B: Polym. Phys.* **2018**, *56*, 9–30.

(85) Ediger, M. D.; Forrest, J. A. Dynamics near Free Surfaces and the Glass Transition in Thin Polymer Films: A View to the Future. *Macromolecules* **2014**, *47*, 471–478.

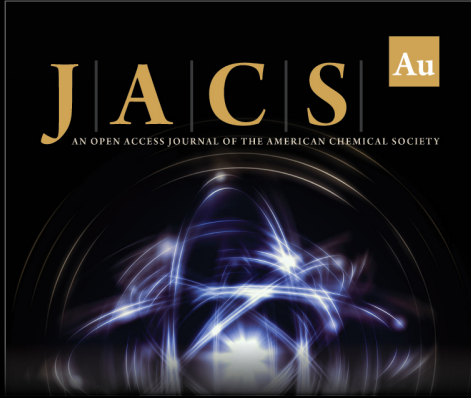
(86) Gomopoulos, N.; Cheng, W.; Efremov, M.; Nealey, P. F.; Fytas, G. Out-of-Plane Longitudinal Elastic Modulus of Supported Polymer Thin Films. *Macromolecules* **2009**, *42*, 7164–7167.

(87) Liu, B.; Pavlou, C.; Wang, Z.; Cang, Y.; Galiotis, C.; Fytas, G. Determination of the Elastic Moduli of Cvd Graphene by Probing Graphene/Polymer Bragg Stacks. *2D Mater.* **2021**, *8*, No. 035040.

(88) Bay, R. K.; Zarybnicka, K.; Jančář, J.; Crosby, A. J. Mechanical Properties of Ultrathin Polymer Nanocomposites. *ACS Appl. Polym. Mater.* **2020**, *2*, 2220–2227.


(89) Chang, J.; Toga, K. B.; Paulsen, J. D.; Menon, N.; Russell, T. P. Thickness Dependence of the Young's Modulus of Polymer Thin Films. *Macromolecules* **2018**, *51*, 6764–6770.


(90) Wang, G.; Dai, Z.; Xiao, J.; Feng, S.; Weng, C.; Liu, L.; Xu, Z.; Huang, R.; Zhang, Z. Bending of Multilayer Van Der Waals Materials. *Phys. Rev. Lett.* **2019**, *123*, No. 116101.



**JACS** Au  
AN OPEN ACCESS JOURNAL OF THE AMERICAN CHEMICAL SOCIETY

Editor-in-Chief  
**Prof. Christopher W. Jones**  
Georgia Institute of Technology, USA

**Open for Submissions** 

pubs.acs.org/jacsau  ACS Publications  
Most Trusted. Most Cited. Most Read.